# 3.
# COMPACT MULTIBAND PLANAR MONOPOLE ANTENNA FOR SLIM MOBILE HANDSET

## 3.1 Introduction

With the rapid growth in the mobile handset technology for communication systems there is always demand for compact thin profile antennas with multiband as well as broadband functionality so that it can be easily accommodated in the ultra-slim mobile handsets. The multiband antennas can operate over different frequency bands used for increasing number of applications for modern handsets which include real time speech communication, text message service, internet surfing, global positioning system (GPS), games, audio and video applications, etc. Therefore, use of multiband and broadband antennas can minimize the problem of placing multiple antennas for different applications.

Design of simple, compact, and low cost multiband antennas for mobile phone applications, which can be easily accommodated with mobile handset circuitry without affecting the other performances of antenna, is a great challenge to antenna designers. However, limitation of size in mobile handsets make it difficult to design antenna with good impedance matching and radiation performances over a number of operating bands which leads the antennas with narrow bandwidth and low return loss level. Therefore, mobile handset antennas are designed to have a minimum reflection coefficient value of −6 dB in the operating bands which is generally low compared to other applications [Seko and Correra (2013)].

Keeping pace with the rapid development of modern mobile communication, several multiband antennas for mobile handset applications have been reported, such as inverted-F antennas (IFA) [Kuo and Wong (2002), Chiu and Chi (2009), Rao *et al.* (2003)], planar inverted-F antennas (PIFA) [Rhyu *et al.* (2009), Anguera *et al.* (2010), Lin *et al.* (2010), Meshram *et al.* (2012), Agarwal *et al.* (2013), folded chip antennas [Chi and Wong (2008), Chiu *et al*. (2010), Peng *et al*. (2011)], and monopole antennas [Wong et al. (2003), Sim *et al*.

(2005), Jing and Gong (2006), DU *et al*. (2006), Li *et al*. (2008), Chen *et al*. (2008), Hsieh *et al*. (2009),Liao *et al*. (2010) Kang and Du (2011), Asghar *et al*. (2013), Sultan *et al*. (2013)]. Though, PIFA and IFA are compact antennas with quarter wavelength structures, suitable for conventional mobile handsets but they have some inherent disadvantages like these antennas are designed on some height in addition to the substrate thickness and they consist of shorting plate/pin which adds to antenna design complexity. Folded chip antennas also have some design complexities like they generally employed two layers of radiating structures and the layers are generally connected through shorting pins or other structures. Therefore, planar monopole antennas are suitable for ultra-slim mobile phones and it has compact quarter wavelength resonating structure with planar geometry which can be easily etched during the fabrication of printed circuit board (PCB) of mobile phones.

Although, several monopole antennas have been reported in literature but they have some demerits that make them unsuitable for modern handsets with lot of applications. In [Wong *et al*. (2003), Chen *et al*. (2008)], simple planar multiband monopole antennas are proposed that covers all the frequency bands that can be utilized for the conventional mobile phone but they do not cover either WLAN or WiMAX bands which are very important in modern day handsets. Similarly, in [Sim *et al*. (2004), Li *et al*. (2008), Kang and Du (2011)], monopole antennas for mobile handsets have been proposed but these antennas do not operate over any of communication bands below 1 GHz which is also a great disadvantage for recent applications whereas, antenna proposed in [Shin *et al*. (2005)] does not have planar structure. The monopole antennas proposed in [Jing *et al*. (2006), Du *et al*. (2006)] do not operate over WiMAX frequency band. While, [Hsieh *et al*. (2009), Asghar *et al*. (2013), Sultan *et al*. (2013)] cover almost all the frequency bands with planar and simple structure but they have limitation in terms of the area occupied by the antenna structure on the mobile circuit board.

In this chapter, a compact, multiband, uniplanar monopole antenna which covers GSM900/ GSM1800/ GSM1900/ UMTS/ IMT2100/ WLAN/

LTE2500/WiMAX frequency bands along with all the higher LTE (Long Term Evolution) frequency bands is proposed. To achieve multiband operation of the antenna, combinations of C-shaped and meandered line embedded with L-strip multi resonating branches are used. The comparison of the proposed antenna with the existing antennas [Hsieh *et al*. (2009), Asghar *et al*. (2013), Sultan *et al*. (2013)] is given in Table 3.1. The details of antenna design concepts and characterization are discussions in following sections.

## 3.2 Antenna Design and Configuration

The configuration of the proposed antenna with fabricated prototype for the ultra-slim mobile handset applications is shown in Fig. 3.1. This antenna consists of two resonating branches (a C-shaped and a meandered line connected with L-strip), 50 Ω microstrip line, and a mobile circuit board. The mobile circuit board is made of FR4 substrate with dielectric constant 4.4 and loss tangent 0.018. The dimension of the circuit board is chosen as 50×110 $mm^2$ with height ($h$) of the substrate 0.8mm. Fig. 3.2 shows the details of the proposed antenna which is printed on the no ground portion of size 15×50 $mm^2$ on one side of the circuit board which is fed by 50 Ω microstrip line, printed on the same side of the antenna whereas the ground plane of size 50×95 $mm^2$ printed on the opposite side of the antenna.

**Table 3.1:** Comparison of proposed antenna with reference antennas.

| Antenna | Frequency bands covered | Antenna size ($mm^2$) | Area occupied by antenna ($mm^2$) | Substrate material used | Substrate thickness (mm) |
|---|---|---|---|---|---|
| [Hsieh *et al*. (2009)] | GSM900/GPS/DCS/PCS/UMTS/ Bluetooth/WLAN/WiFi/WiMAX | 30 × 35 | 1050 | FR4 ($\varepsilon_r$=4.4) | 1.6 |
| [Asghar *et al*. (2013)] | LTE750/GSM850/GSM900/DCS/ UMTS-2110/Bluetooth/WLAN/ WiMAX/UWB | 17.6 × 55 | 968 | Rogers 4360 ($\varepsilon_r$=6.15) | 0.305 |
| [Sultan *et al*. (2013)]* | GSM850/GSM900/DCS1800/ PCS1900/UMTS2100/ISM2450/WLAN/ WiMAX/most LTE bands | 33 × 25 | 825 | FR4 ($\varepsilon_r$=4.4) | 0.8 |
| Proposed | GSM900/GSM1800/GSM1900/ UMTS/IMT2100/ WLAN/WiMAX/LTE | 15 × 50 | 750 | FR4 ($\varepsilon_r$=4.4) | 0.8 |

* Actual mobile circuit board size ground plane is not considered for antenna design and characterization

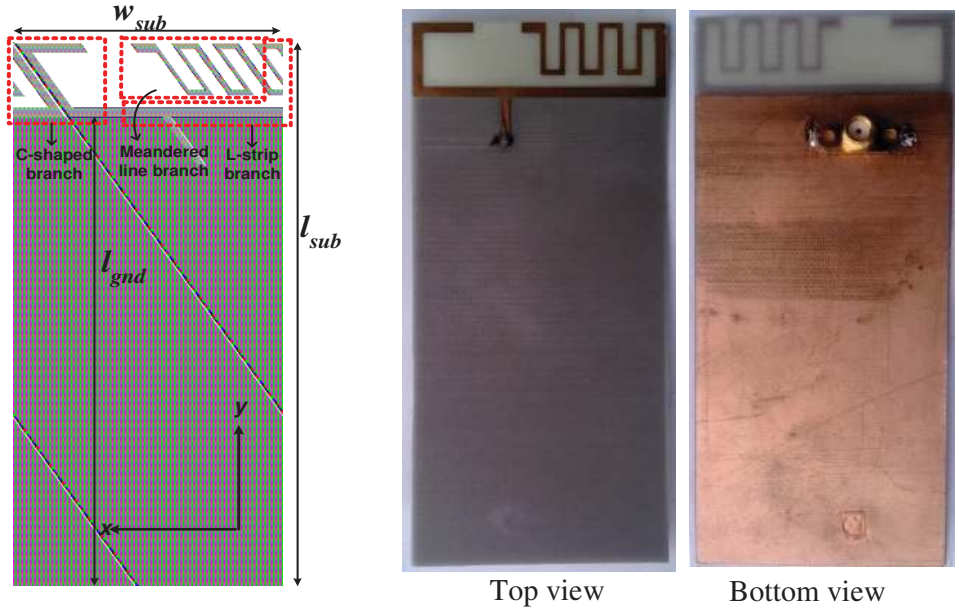


**Fig. 3.1:** The configuration of the proposed antenna with fabricated prototype.

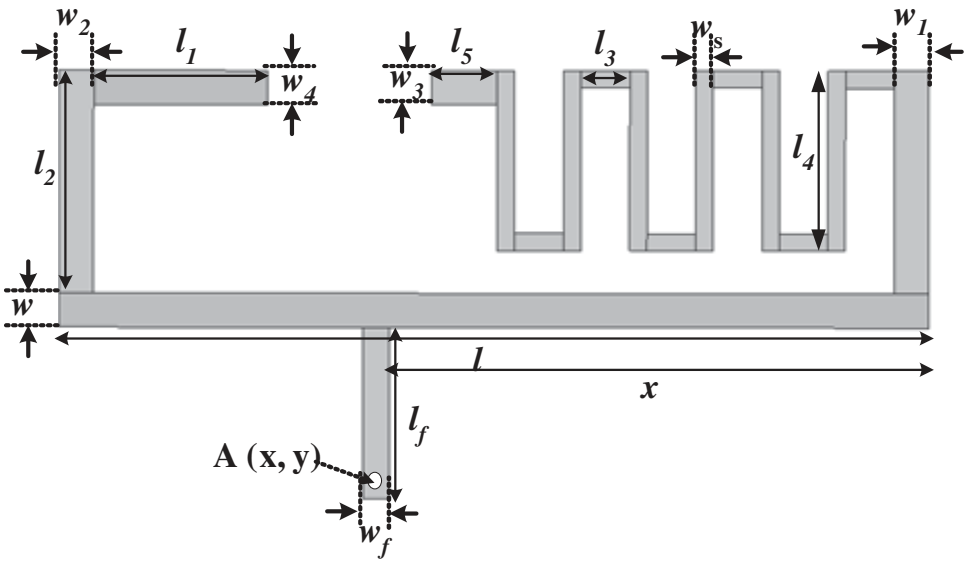


**Fig 3.2:** Detail dimensions of the proposed antenna.

The electrical length of the meandered line branch is approximated as 3λ/8 at the lowest resonant frequency [Chen and Peng (2011)]. C-shaped branch is responsible for the higher frequency bands. The electrical length of the C-shaped branch can be approximated as λ/4 at lower edge operating frequency of the higher frequency band.

Since the proposed antenna comprises of two resonating branches. It is interesting to see the effect of individual branch on the impedance bandwidth of the antenna. When both the branches are considered separately on the same circuit board, the meandered line strip connected with L-shaped strip (case 2) has fundamental (3/8) λ resonating mode near 0.94 GHz with other higher order modes resonating at 2.7 GHz and 3.8 GHz, while the quarter wavelength C-shaped strip (case 1) resonates over wide frequency band from 1.9 GHz to 3.825 GHz. When both the branches are combined to form the proposed antenna, then due to coupling between both the branches result in shift of resonance frequencies towards lower frequency side and the impedance bandwidth covers most of the frequency bands used in modern mobile handset applications, which is depicted in Fig. 3.3.

The shape parameters of the antenna are optimized using FEM (Finite Element Method) based Ansoft's HFSS, to achieve the GSM900 (0.885 GHz–0.962 GHz) and higher LTE bands along with GSM, UMTS, IMT 2000, WLAN, and WiMAX bands (1.69 GHz–3.8 GHz). GSM900 and 1.69 GHz–3.8 GHz are referred as lower and higher frequency bands, respectively in this chapter. The optimized shape parameters of proposed antenna are shown in Table 3.2.

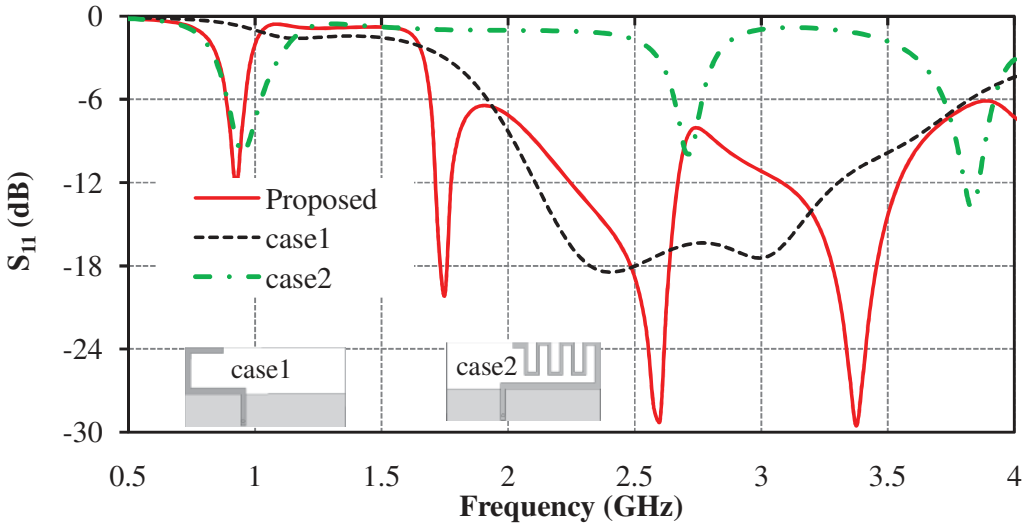


**Fig. 3.3:** Variation of reflection coefficient with frequency for different configurations.

**Table 3.2:** Optimized shape parameters of the proposed antenna

| Parameters | Value (mm) | Parameters | Value (mm) |
|---|---|---|---|
| $w_{sub}$ | 50 | $w$ | 2 |
| $l_{sub}$ | 110 | $w_s$ | 1 |
| $l_{gnd}$ | 95 | $w_1$ | 2 |
| $l$ | 50 | $w_2$ | 2 |
| $l_1$ | 10 | $w_3$ | 2 |
| $l_2$ | 13 | $w_4$ | 2 |
| $l_3$ | 2.8 | $x$ | 31 |
| $l_4$ | 10.5 | $w_f$ | 1.5 |
| $l_5$ | 3.75 | $l_f$ | 10 |
| A(x, y) | (31.75, 86.5) | | |

## 3.3 Antenna Characterization in Free Space

The simulations are performed originally in Ansoft's HFSS to optimize the antenna parameters for the desired operating bands.

### *3.3.1 S-Parameter Characterization*

In this section *S*-parameter of the proposed antenna is investigated for the different shape parameters to see the effect on the impedance bandwidth. Thereafter, the simulated results are compared with the measured result.

#### *3.3.1.1 Parametric analysis*

Parametric study of some critical dimensions of the antenna is carried out to analyze the effect of the shape parameters on the operating frequency bands using HFSS. The antenna is designed to cover the GSM900 (0.885 GHz–0.962 GHz) and higher LTE bands along with GSM, UMTS, IMT 2000, WLAN, and WiMAX bands (1.69 GHz–3.8 GHz).

The effect of variation of $l_1$ on impedance bandwidth is shown in Fig. 3.4. It is observed that, with the increase of the length $l_1$, resonant frequency around 2.5 GHz decreases rapidly whereas almost unaffected around 3.5 GHz and 1.8 GHz. Also slight increase on the lower edge frequency of the higher frequency band is observed. The impedance bandwidth ($S_{11} \leq -6$ dB) of higher frequency side does not get affected significantly but the impedance matching around 3 GHz and 2.7 GHz reduces while around 2 GHz get improved. Since the length of quarter wavelength C-shaped strip is responsible for resonating mode around 2.4 GHz and 3 GHz, therefore shifting of resonant frequency around 2.5 GHz towards lower frequency side take place while mismatch occur around 3.4 GHz.

The effect of variation of length $l_3$ is shown in Fig. 3.5. It is observed that with the increase of length $l_3$, the resonant frequency around GSM 900, 2.5 GHz, and 3.5 GHz decreases while the resonant frequency around 1.8 GHz is unaffected. This 1.8 GHz resonant frequency is fundamental resonating mode at $\lambda/4$ length of C-shaped strip, hence it is unaffected due to change in the length of meandered section. Similar behavior is observed with the variation of length $l_5$ since it directly affects the total length of the branch.

Further, the effect of variation of the length $l_4$ is investigated which is shown in Fig. 3.6. It is observed that with the increase of length $l_4$ the effective electrical length of meandered line section increases and the gap between the meandered line sections with L-strip line decreases which results in shifting of the resonant modes towards lower frequency side while improvement in impedance matching is observed at higher frequency side.

The effect of variation of the feed position $x$ is shown in Fig. 3.7. It is observed that the position of the feed affect the impedance matching significantly specially at the higher frequency side with less effect on the lower frequency bands. The optimized value for the feed position is considered as 31mm.

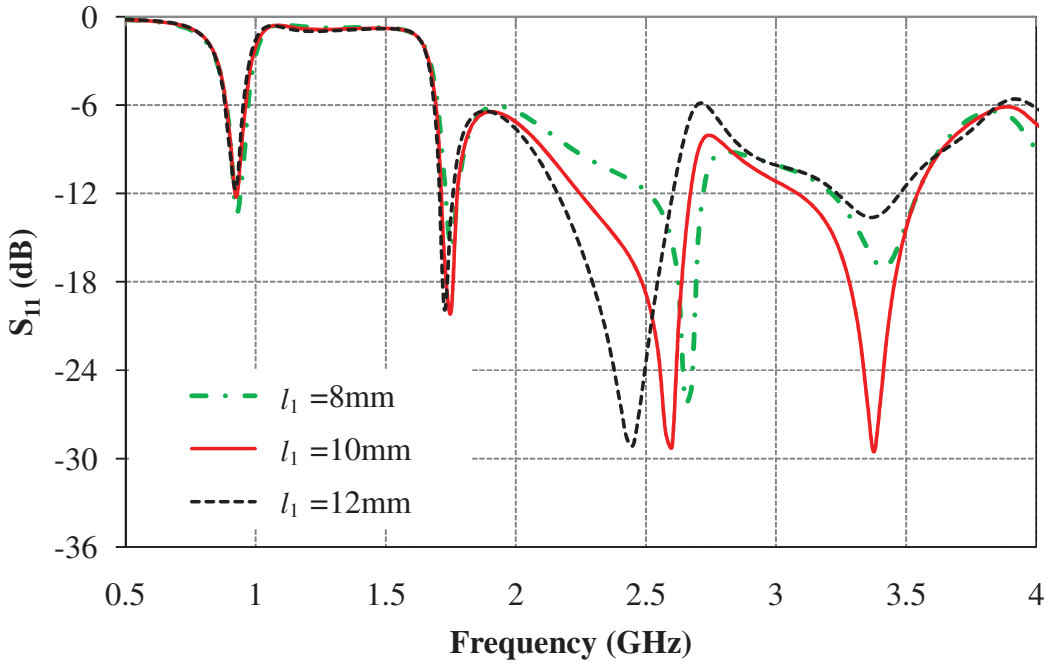


**Fig. 3.4:** Variation of reflection coefficient with frequency for $l_1$.

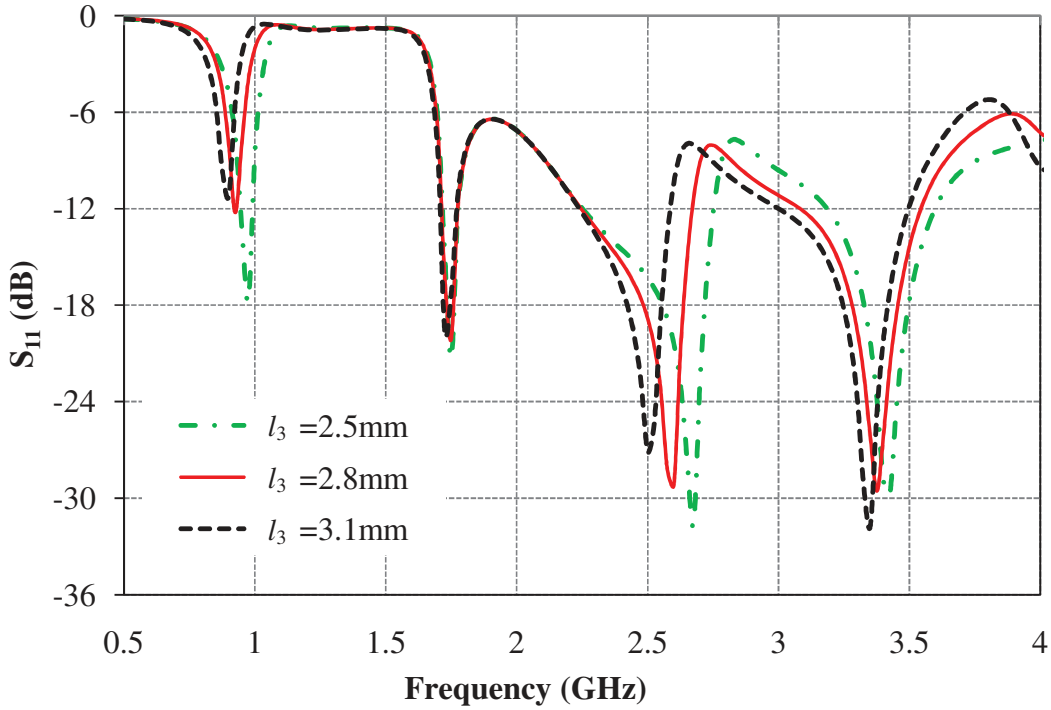


**Fig. 3.5:** Variation of reflection coefficient with frequency for $l_3$.

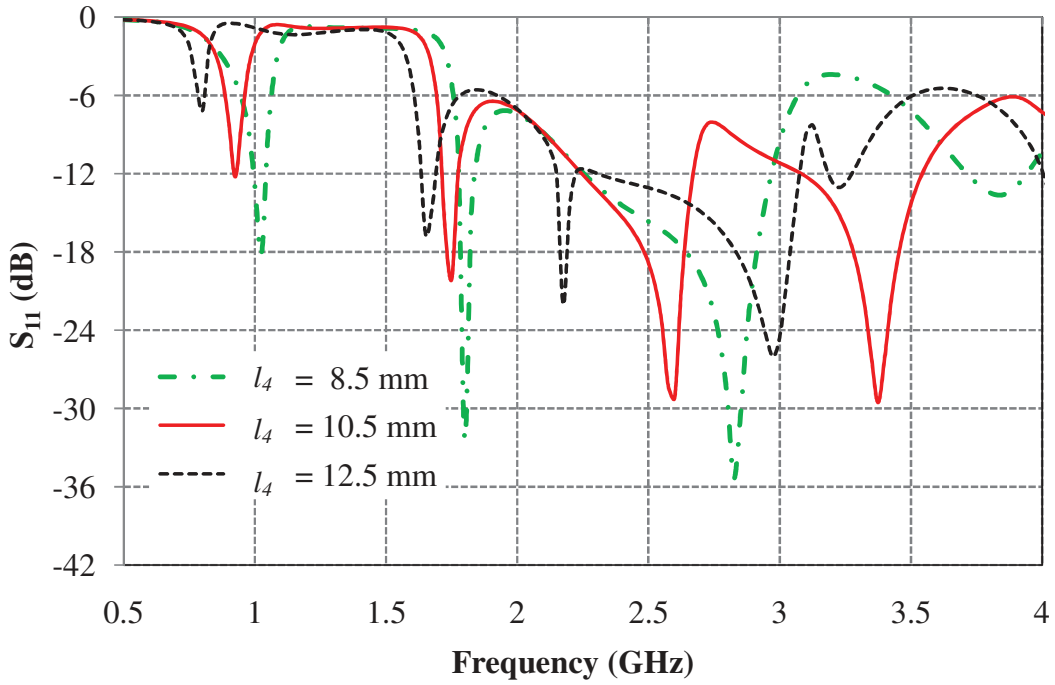


**Fig. 3.6:** Variation of reflection coefficient with frequency for $l_4$.

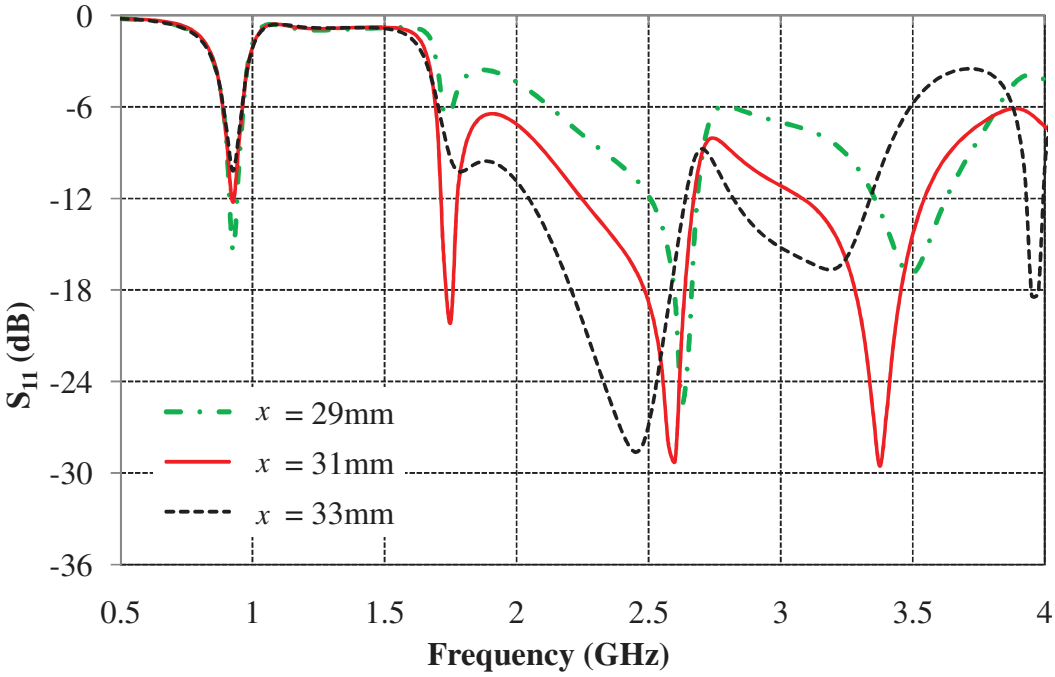


**Fig. 3.7:** Variation of reflection coefficient with frequency for $x$.

The variation of the width of the feed line ($w_f$) and the height of the substrate ($h$) with frequency are shown in Fig. 3.8 and 3.9, respectively. It is observed that the variation of feed line width has significant effect on impedance bandwidth towards higher frequency side while less significant effect at lower frequency side, whereas the variation of height of the substrate significantly affects the overall impedance bandwidth. It is observed that with the increase of $h$ all the resonance frequency points are shifted towards the lower frequency side with some impedance mismatch with respect to −6dB impedance bandwidth.

The effect of variations of $w_s$, $w_2$, $w_4$, and $w$ on impedance bandwidth is shown in Fig. 3.10, 3.11, 3.12, and 3.13, respectively. It is observed that with the increase of $w_s$, the lower frequency band is not affected significantly while the resonant frequencies of the higher frequency band increases with some impedance mismatching around 3.0 GHz frequency. It is interestingly noted that the impedance matching improved after 3.5 GHz with the increase of $w_s$. It is worth mentioning that during the simulation process we observed that the value of width $w_1$ does not influence significantly the reflection coefficient as well as the impedance bandwidth of the antenna. Also, it is observed that the reflection coefficient and impedance bandwidth remains almost unaffected by the variation of the width $w_3$.

Since $w_2$ and $w_4$ are related to C-shaped strip which is responsible for higher operating bands, therefore with the increase of $w_2$ the significant effect is observed at higher frequency side with the improved impedance matching. The resonant frequencies of the higher frequency band decreases with the increase of $w_4$ while lower frequency band is almost unaffected. The variations of the width $w$ affect the impedance matching significantly at both the lower and higher frequency bands. With the increase of $w$ the impedance matching improve significantly at lower frequency band with slight shift towards higher side while at higher frequency band the lower edge operating frequency shift towards higher value with some impedance matching throughout the band.

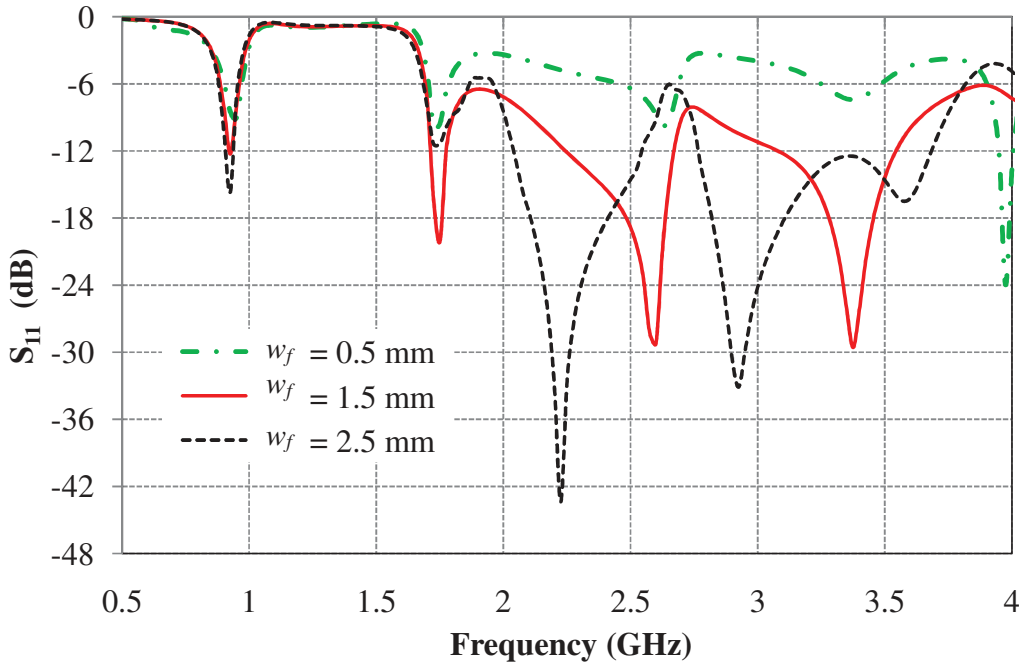


**Fig. 3.8:** Variation of reflection coefficient with frequency for $w_f$.

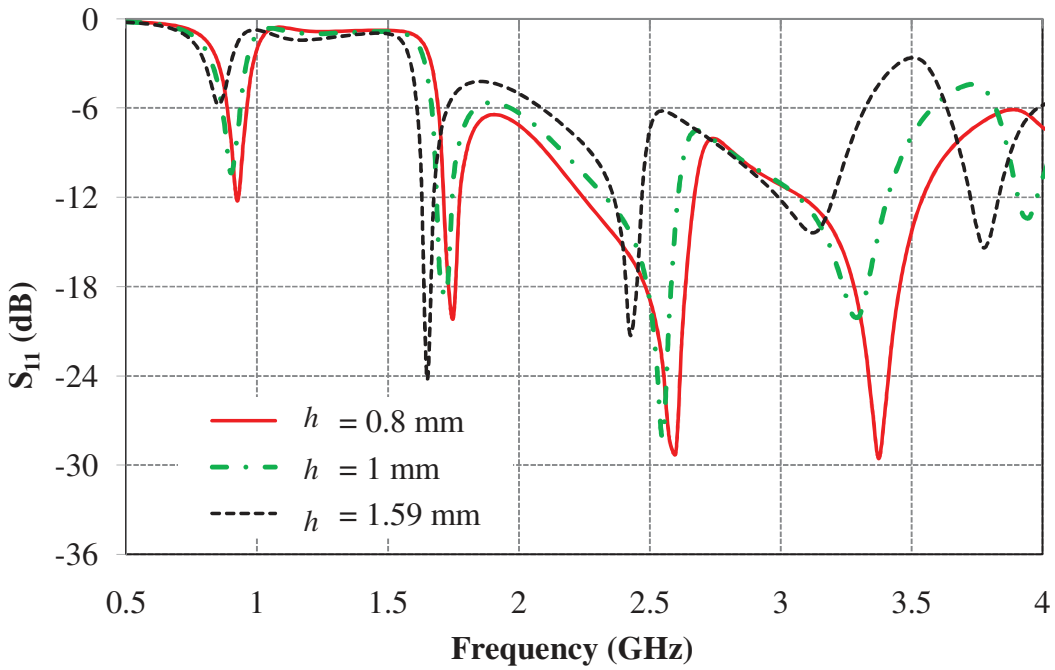


**Fig. 3.9:** Variation of reflection coefficient with frequency for $h$.

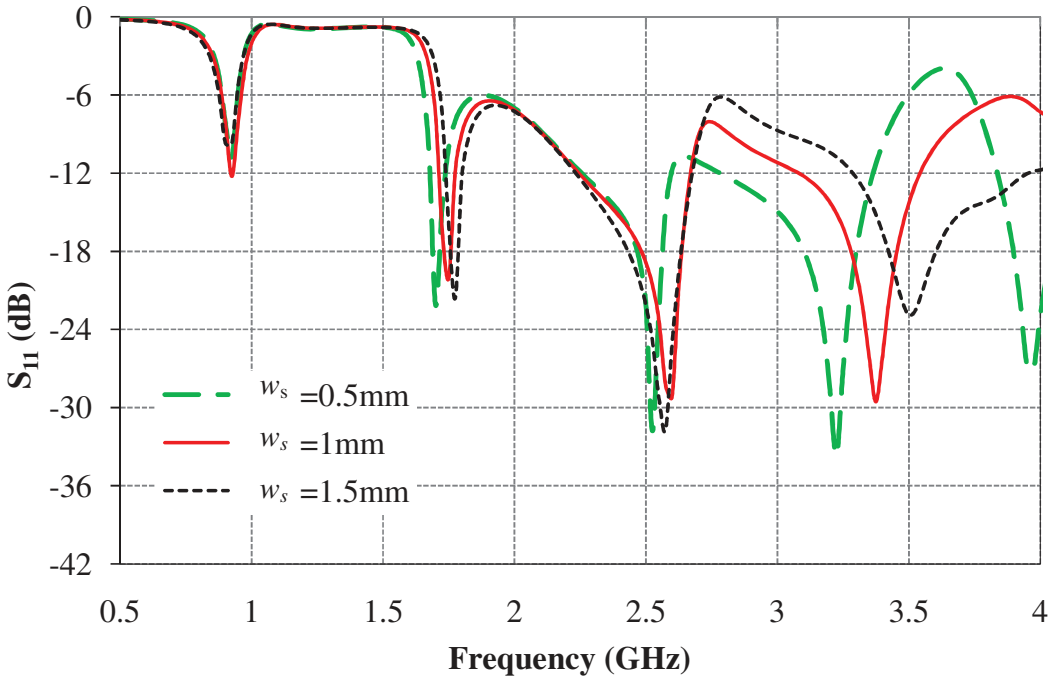


**Fig. 3.10:** Variation of reflection coefficient with frequency for width $w_s$.

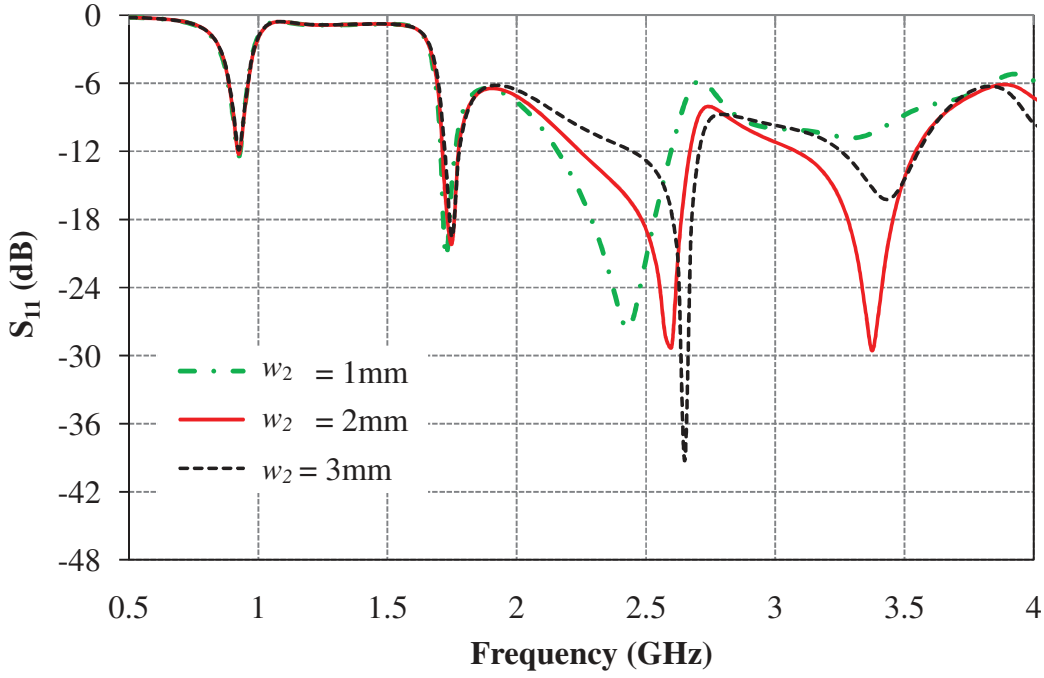


**Fig. 3.11:** Variation of reflection coefficient with frequency for width $w_2$.

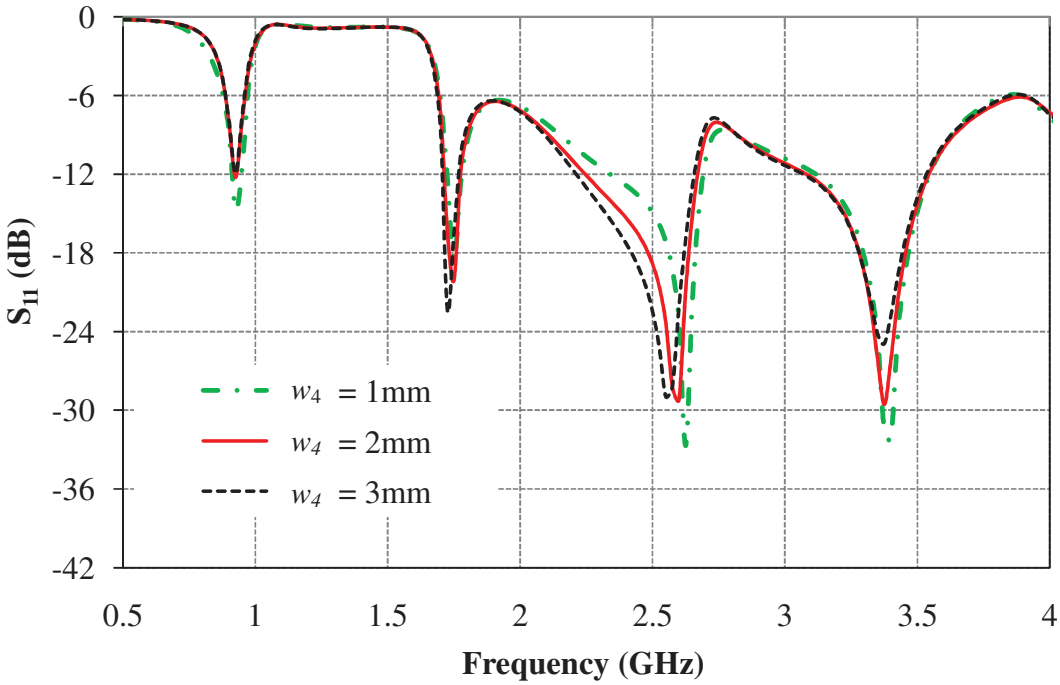


**Fig. 3.12:** Variation of reflection coefficient with frequency for width $w_4$.

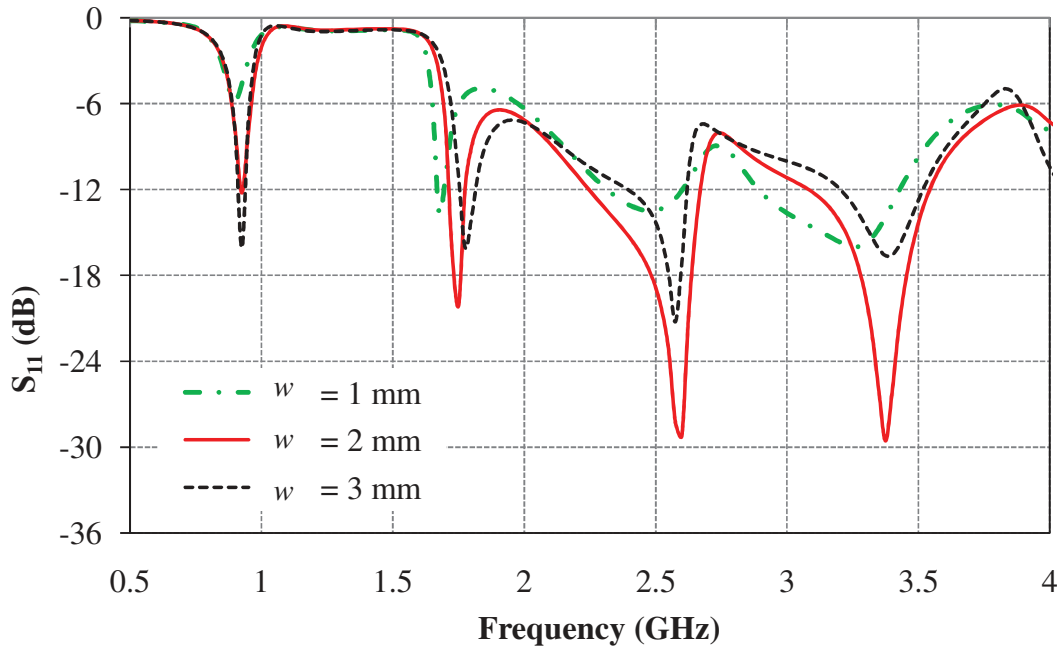


**Fig. 3.13:** Variation of reflection coefficient with frequency for width $w$.

### *3.3.1.2 Measurement of S-parameter*

A prototype of the optimized antenna is fabricated using T-Tech QC5000 micro-milling machine. The characteristics of the fabricated prototypes are measured with the help of Anritsu VNA Master MS2038C. The simulated results of HFSS are compared with the measured and simulated results of CST Microwave Studio (CST MWS) of the antenna operating in free space. Variation of reflection coefficient of the proposed antenna with frequency in free space is shown in Fig. 3.14. It is observed that the measured and simulated results are in good agreement. It is also observed that with reference to −6 dB reference level, the antenna operates over the prerequisite frequency bands.

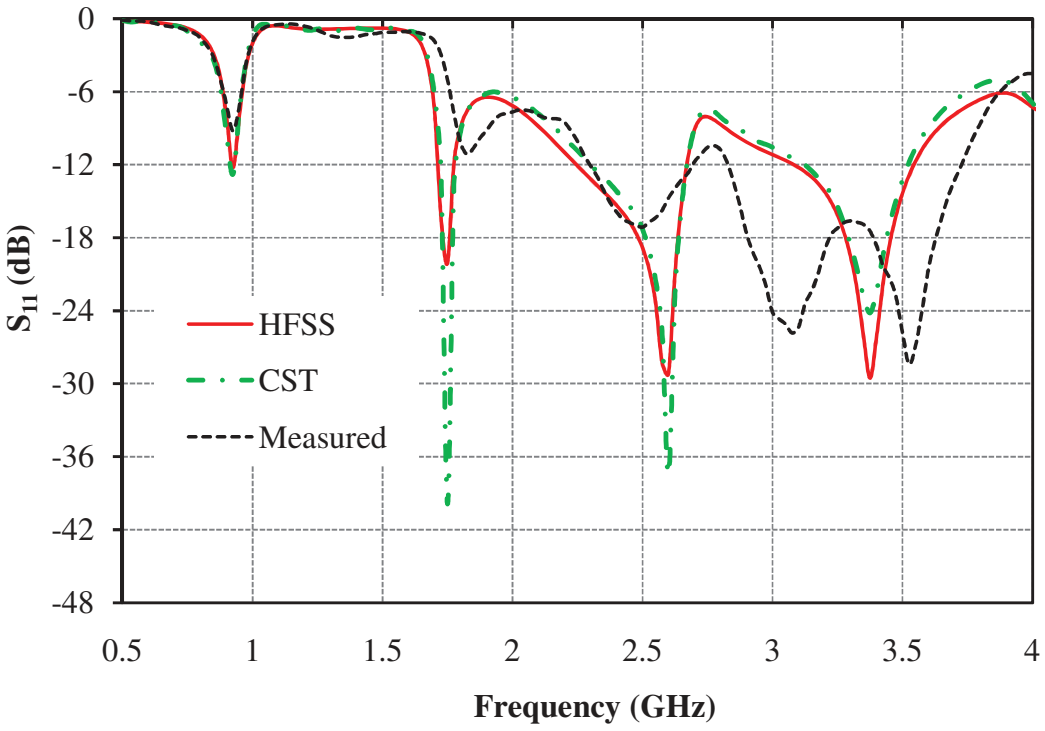


**Fig 3.14:** Variation of reflection coefficient of the proposed antenna.

### *3.3.2 Surface Current Distributions*

To understand the radiation mechanism of the proposed antenna, the simulated surface current distributions on the proposed antenna at different frequencies (0.925 GHz, 1.925 GHz, 2.45 GHz, and 3.5 GHz) are presented in Fig. 3.15 (a). At 0.925 GHz, the relatively strong current distributions are seen on the meandered line and L-strip sections, which indicates that dominant mode is excited and lower resonant mode at about 0.925 GHz is mainly contributed by these sections. It is also observed from Fig. 3.15 (b), (c), and (d) that there are strong surface current distributions on the meandered line, L-strip , and C-shaped strip sections, which suggests that resonant modes at 1.925 GHz, 2.45 GHz, and 3.5 GHz frequencies are provided by all these sections.

### *3.3.3 Far Field Radiation Characteristics*

The radiation characteristics of proposed antenna in three principal planes are shown in Fig. 3.16. It is observed that the $E_\theta$-component makes dumbbell like shape in XY- and YZ-plane and close to omni-directional pattern in XZ-plane for all the resonant frequencies. It is interestingly noted that at 0.925 GHz and 2.45 GHz in Fig. 3.16 (a) and 3.16 (c) respectively, the $E_\theta$-component of the field is dominant and provides smooth variations over all the $\theta$ angles which can be seen in XZ-plane. This is due to dominant mode is excited at 0.925 GHz and favorable higher order mode is excited at 2.45 GHz, which can be seen from the current distributions on aperture as shown in Fig. 3.15 (a) and 3.15 (c), respectively. However, at 1.925 GHz and 3.5 GHz in Fig. 3.16 (b) and 3.16 (d) respectively, $E_\theta$-component of field is not varying uniformly over all the θ angles, two nulls can be seen in both the frequencies at $\theta$ angles of 30 and 150 degrees and at 210 and 330 degrees respectively, which are due to the generation of unfavorable higher orders modes as indicated from current distributions in Fig. 3.15 (b) and 3.15 (d), respectively. In YZ-plane, $E_\varphi$-component of field is dominant and having almost uniform variations over all $\varphi$ angles. Comparable $E_\theta$ and $E_\varphi$ components are seen in all the three principal planes resulting into elliptical polarization. In mobile application, there is a significance of total field rather than one component, so

even though the vertical component variation is not uniform, an addition of both the vertical and horizontal component gives the fairly good angular coverage.

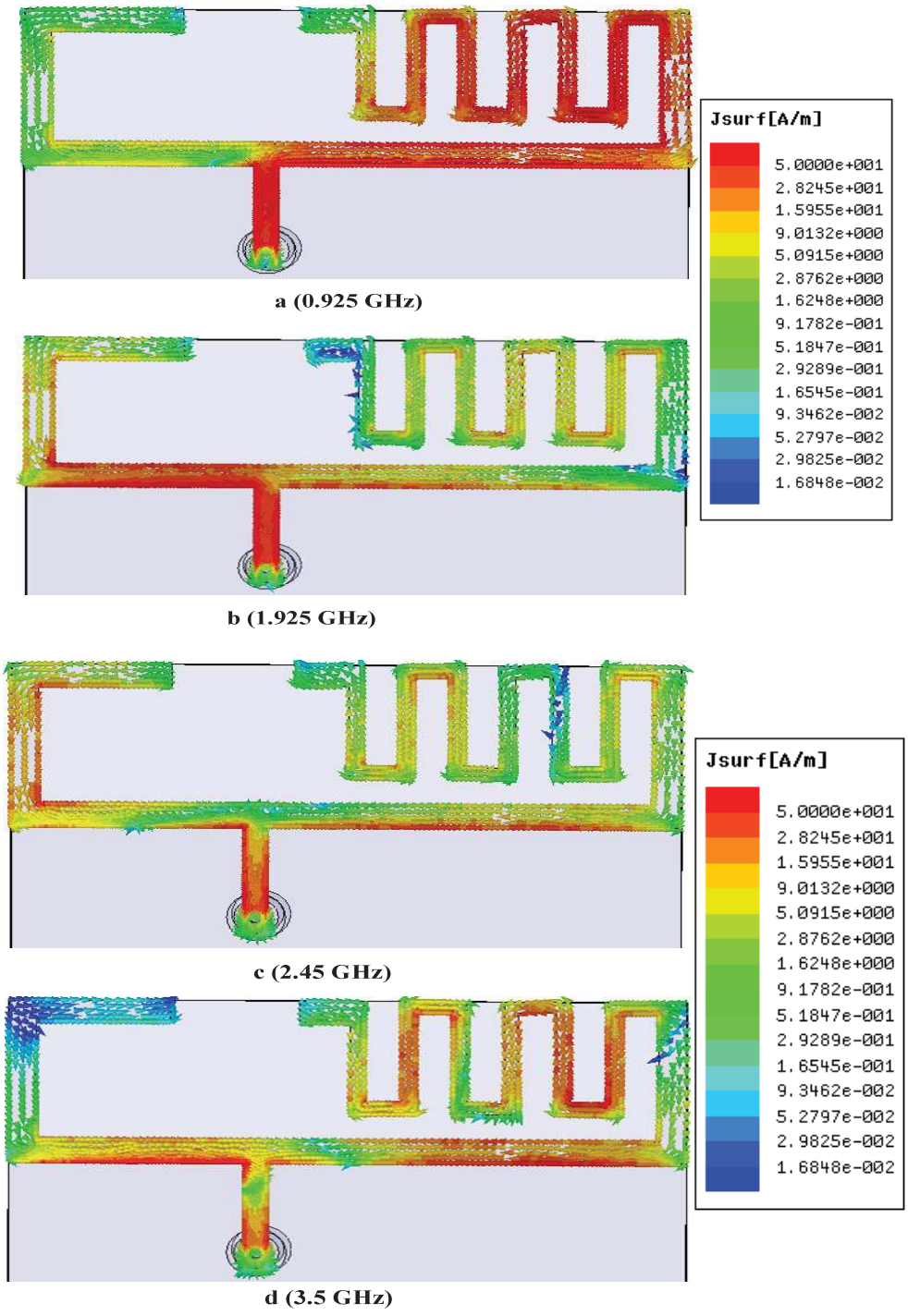


**Fig. 3.15:** Surface current distributions of proposed antenna at different frequencies.

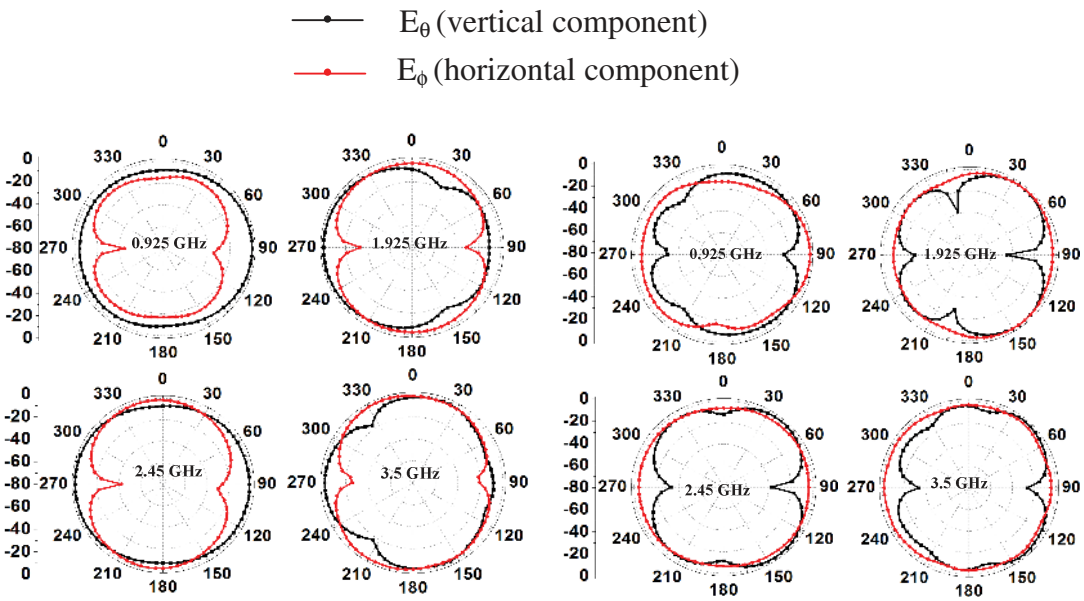


**(a)** **(b)**

**X-Y Plane (Theta = 90$^o$ and Phi = all)** **Y-Z Plane(Theta = all and Phi =90$^o$)**

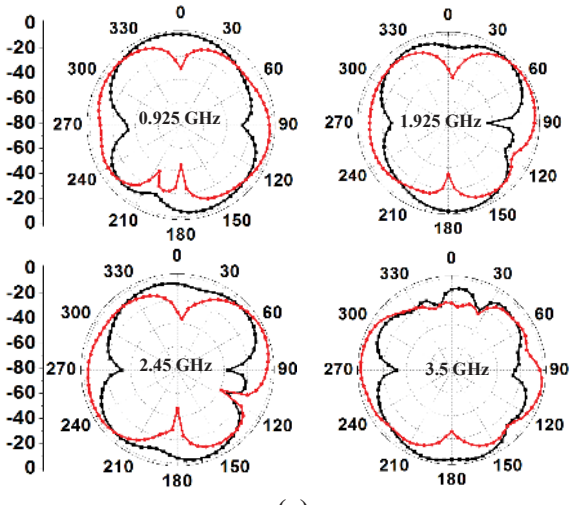


**(c)**

**X-Z Plane(Theta = all and Phi =0)**

**Fig. 3.16:** The radiation patterns of proposed antenna at different frequencies.

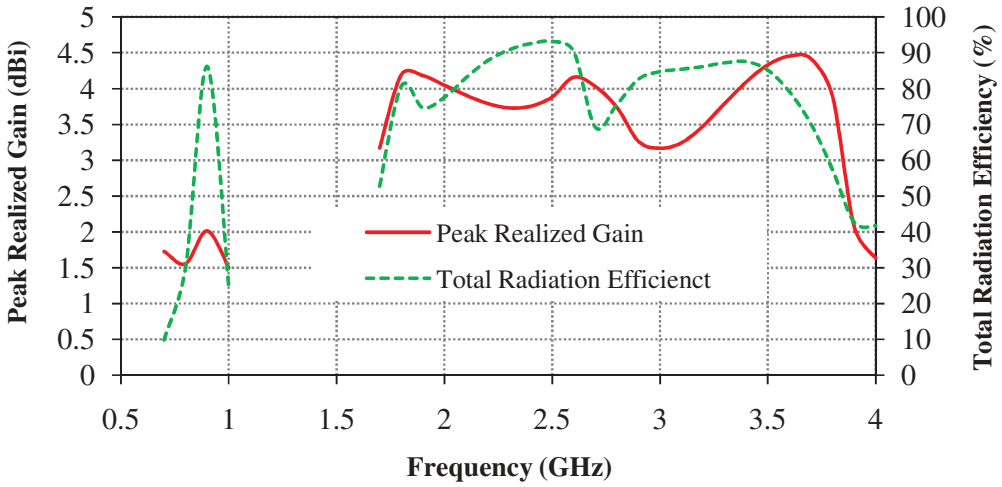


**Fig. 3.17:** Variation of peak realized gain and total radiation efficiency.

The calculated peak realized gain and efficiency variation with frequency are shown in Fig. 3.17. The minimum peak realized gain value is found to be 1.5 dBi at lower frequency (0.885 GHz) and as the frequency increases the peak realized gain increases and maximum value of the gain is found to be 4.5 dBi about 3.7 GHz. The total radiation efficiency of the antenna lies in the range of 73% to 93% in the operating frequency bands which show good radiation characteristics.

## 3.4 Antenna Characterization in Mobile Environment

The proposed antenna is also investigated in vicinity of the mobile environment. Mobile environment is made of the plastic housing (60×120×14.3 $mm^3$), LCD display (48×80×2 $mm^3$), and the battery (33.5×50.5×4 $mm^3$). A setup is designed in Ansoft's HFSS as shown in Fig. 3.18. The battery and LCD are assumed as a PEC (Perfect Electric Conductor) material. The battery is placed on the top of the substrate where antenna is fabricated and LCD is placed on the bottom side of the substrate (towards ground plane), the components have air-gap of 1mm from surface of the substrate. Both the components are connected to the substrate with metallic connecting pins provided at the ends of the components. Further, the positions of connecting pins which connect the LCD or battery to the PCB are also a critical parameter to be analyzed. Therefore, some cases are studied like when connecting pins are only provided either of the ends of the

components such as either antenna side or far from the antenna side and when the connecting pins are present at the both ends of the components. Fig. 3.19 shows the variation of reflection coefficient with frequency for antenna in free space and in the mobile vicinity with different components and connecting pins. It is observed that there is shifting of the resonating bands towards lower frequency side for both the lower and higher frequency bands in all the cases. Less significant effect is observed on the overall impedance matching. Therefore, it can be concluded that there is no significant effect observed on the performance of the antenna in the mobile environment.

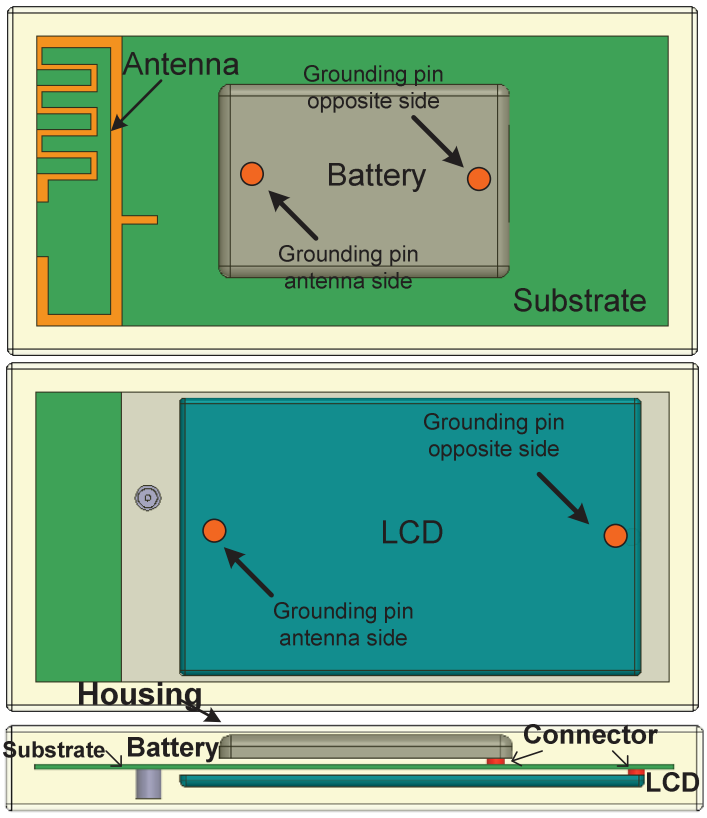


**Fig. 3.18:** Antenna in mobile environment

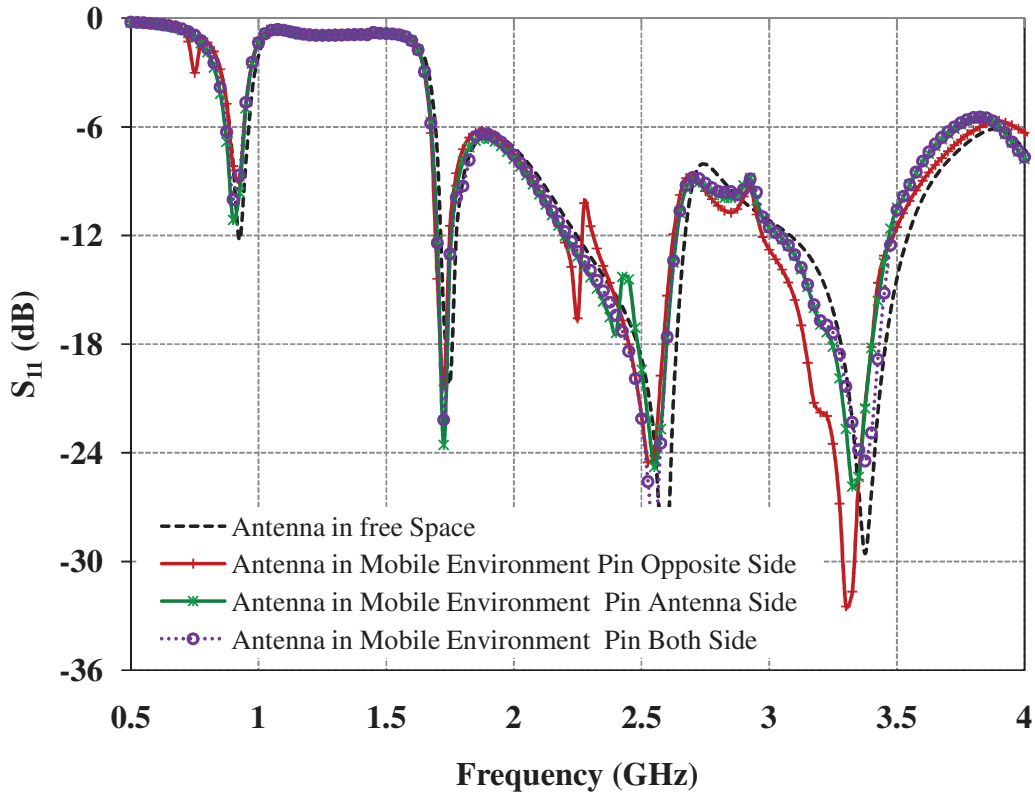


**Fig. 3.19:** Effect of mobile environment on *S*-parameters

After completing the study on compact multiband planar monopole antenna for slim mobile handset applications, the investigations on multiband shorted monopole antenna for slim mobile handset application is taken up in details in the following chapter four.